

# **On the frequency dependency of fatigue damage caused by viscous fluid-structure interaction in hydraulic components**

Lukas Michiels and Marcus Geimer

Institute of Mobile Machines, Karlsruhe Institute of Technology, Karlsruhe, Germany  
E-mail: lukas.michiels@kit.edu, marcus.geimer@kit.edu

## **Abstract**

Experimental fatigue tests have been conducted for decades to study the lifetime of hydraulic components. Nevertheless, predicting the lifetime of hydraulic components remains difficult. For a quick market entry, test periods have to be short, and tests are often done under constant cyclic loading at high frequencies. The damage accumulation of hydraulic components, however, depends on the temporal load profiles, as viscous fluids introduce a time dependency. As a result, high pulsation frequencies alter the damage accumulation, which can result in misleading and inapplicable lifetime results. Previous studies have shown a significant difference in crack growth and lifetime when specimens have been submerged in pressurized oil. Despite the similarities between these experiments and hydraulic systems, the frequency dependency of fatigue damage in hydraulic components and the corresponding fluid-structure interaction in fatigue cracks have not yet been quantified. A one-dimensional numeric flow model in connection with a finite-element structural analysis was used to simulate the fluid flow and the crack opening. Based on the resulting stress amplitudes, the expected crack growth was predicted and compared to experimental data. The experiments show that the temporal load profile is critical to ensure equivalent damage accumulation in fatigue experiments. Otherwise, premature component failures can occur, and a large safety margin has to be applied.

**Keywords:** Damage accumulation, Fatigue, Hydraulics, Mobile Machines

## **1 Introduction**

In many applications, hydraulic power systems are subject to cycling or transient loads, resulting in a significant number of load cycles over the components' lifetime. Under cyclic load conditions, material fatigue is limiting the lifetime. Therefore, hydraulic power systems must be thoroughly tested in order to avoid premature system failure.

In contrast to static failure due to a single overload, fatigue occurs at much lower stress thresholds. Fatigue damage is caused by small defects or cracks which propagate due to cyclic loading. The material strength depends on the applied stress amplitude. At high stress rates, low-cycle fatigue occurs, which leads to rapid failure after roughly  $10^4$  cycles. On the other extreme, for stress amplitudes below the fatigue strength failures are not to be expected before  $10^7$  load cycles. The most important area in practice is, however, the high-cycle-fatigue, where component's lifetime is sufficient for most applications and a lightweight, and efficient design is possible. The service life of components can be generally divided into two phases, crack initiation and crack growth, see Figure 1. Stress concentrations are reducing the crack initiation lifetime significantly. When introducing artificial defects at a stress concentration, e.g. in the milling process of notches, the initiation lifetime can be reduced to a minimum. [1]

The crack propagation rate is affected by many aspects. One of them is the ratio of the minimal and maximal stress level. At constant maximal load, increasing the minimal stress level of the crack decreases the stress amplitude and reduces the crack propagation rate, [1]. Besides other mechanisms, viscous fluids can prevent crack closure and increase the minimal stress level, see Figure 2. In the case of oil, the mechanism of fluid introduced crack closure is also denoted as oil trapping. Unlike material fatigue tests, which are nowadays performed in an accelerated process, hydraulic components are mostly tested at low frequencies of up to 3 Hz. Accelerating the fatigue tests in the development of hydraulic components would decrease time to market and development costs. However,

Location of crack initiation	Total lifetime of individual lifetime phases
Crack initiation on a smooth surface	
Crack initiation on a notch (stress concentration)	
Crack initiation on a defect (material defect, welding fault, etc.)	
	

Figure 1: Total service life and phases of service life as functions of the crack initiation position, [1].

accelerated tests are impossible if the crack propagation is frequency dependent. In these cases, accelerated tests would lead to invalid results. When applying high-frequency pressure pulsations to hydraulic components, the compressibility of the fluids can lead to significant volume flows, which introduce a time dependency. While an adequate test layout can ensure homogeneous pressure distribution within the tested specimens, the fluid structure interaction inside fatigue cracks and the consequences on crack propagation are not yet fully understood.

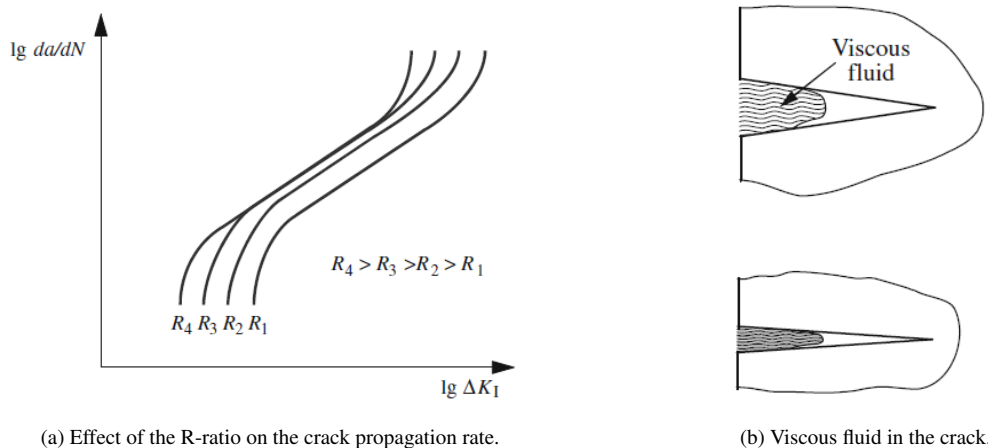


Figure 2: Crack propagation and fluid induced crack closure, [1].

The first experiments regarding the frequency dependency of hydraulic components were performed by Crook in the late 19th century, [2]. The experiments showed a strong increase in the lifetime of gear pumps with increased frequency. The lifetime in terms of cycles was up to ten times higher at a 5 Hz cycle frequency than at a 1 Hz cycle frequency. Because of this magnitude, increasing the frequency further would, at some point, not only increase the lifetime in terms of cycles until failure, but also the overall experiment durations. Crook thus discovered a global minimum in terms of the overall duration of the tests performed. Compared to our experiments, the temporal pressure gradients are assumed to be more or less equal for all frequencies. However, their test specimens have been designed with a relevant wall thickness of 1.05 mm, highly limiting the crack length and the area of fluid-structure interaction.

Davis and Ellision investigated submerged specimens in related fields, [3], [4]. In their experiments, they compared the crack growth of specimens submerged in oil and non-submerged specimens. The submerged specimens showed a slight decrease in the crack propagation rate. Based on these results, they concluded that the hydrodynamic pressure caused by the oil's flow resistance due to its high viscosity opposes crack closure. As the crack is not closing during the low-stress phase, the lower stress level is increased, and the overall stress amplitude is decreased for submerged specimens. Additionally, they compared the crack propagation rates when additional hydrostatic pressure is applied to the submerged specimens. The crack rate increased when hydrostatic pressure was applied. In consequence, the influence of the hydrostatic pressure surpasses the influence of the hydrodynamic pressure and the crack closure. However, it must be assumed that the magnitude of these mechanisms is strongly dependent on

the particular experiment and cannot be generalized. Plumbridge et al. also reported increased crack propagation rates in connection with ambient hydrostatic pressure, [5].

In their experiments, Polk et al. reported lower crack propagation rates in connection with high-viscous fluids, [6]. Tzou et al., on the other hand, conducted experiments that resulted in increased crack growth rates at low fatigue levels, while oil reduced crack growth rates at high fatigue levels, [7]. To explain these differences, they proposed three competitive mechanisms. At low fatigue levels, the dominant mechanism is the suppression of corrosion fatigue, whereas at high fatigue levels, the effect of oil wedging is more dominant. In all of these experiments, the material stress and the structural deformations have been applied externally. However, the load pressure inside the components causes the structural deformation in hydraulics, which is more similar to those experiments. In contrast to hydraulic components, however, the load pressure only acts on the inside of the structure, whereas the ambient pressure in these experiments acts on all surfaces. These differences hinder a direct transfer of the fluid-structure interaction in hydraulic components.

In rolling contacts, fluid penetrations of fatigue cracks is regarded as an important mechanism, [8]. Fluid on the contact surface is pressed into the crack by the surface force. Similar to hydraulics, the surface contact exerts a pressure on the fluid which causes the penetration of the crack. When the movement of the rolling contact is in the direction of the crack, the advancing surface force closes the crack mouth and the oil is trapped inside the crack, leading to an additional stress at the crack tip, [9]. The general assumption of pressurized fluid penetrating the crack and exerting an additional stress is in line with the fluid structure interaction in hydraulic applications.

Fluid flow came to attention with the leak-before-break (LBB) concept for pressurized vessels, [10]. Bagshaw et al. used an idealized crack geometry to study the flow regime in narrow cracks and compared it to laminar and turbulent flow models, [11]. The suggested four flow regimes in dependence of the crack's opening displacement. Whereas a laminar flow regime was established in small cracks, the fluid flow in larger cracks tended to a turbulent flow regime. Clarke et al. measured the fluid flow in the narrow cracks in cracked specimens in an experimental study, [12]. Their results aligned well with a laminar flow model between two plates for cracks, where the crack's opening displacement is larger than the grain size. For smaller cracks however, the actual fluid flow has been significantly higher than the prediction of the laminar flow model.

We demonstrated in [13] that load pressure acts on the crack surface and induces additional mechanical stress, resulting in increased stress amplitudes. The simulations showed that, in particular at low fatigue levels, filling the crack with oil requires a significant amount of time; therefore, it can be doubted that in all the mentioned experiments the cracks have been fully filled with oil during one cycle. The required time should be decreased by ambient pressure. In consequence, two competing mechanisms could be assumed in the experiments with ambient pressure. On the one hand, the ambient pressure leads to higher fill levels in the crack and therefore increased mechanical stress due to the surface pressure. On the other side, the oil inside the crack opposes the crack closure and, as a consequence, leads to lower stress amplitudes. Based on [7], the significance of both mechanisms depends on the fatigue level. Furthermore, we demonstrated in [13] that fast temporal gradients induce high pressure levels at the crack tip, far exceeding the load pressure level. The influence of these increased pressure levels at the crack tip is, however, not yet understood.

In this paper, we used simulation methods to model the fluid-structure interaction in fatigue cracks and calculate the provoked damage to predict the component's lifetime. The experiments were carried out in order to artificially reproduce the described mechanism and compare stable crack growth at various frequencies and temporal gradients. The paper is structured as follows, in Section 2 the two-way coupled dynamic fluid simulation with crack growth calculation is explained. The experimental setup is described in Section 3. This section is subdivided into the description of the test specimens and the test bench. The Section 4 contains the simulation and experimental results, which are discussed in the second part of this section before concluding the paper in Section 5.

## 2 Fatigue Simulation

The fatigue simulation's goal is to predict the cycle count of the tested specimens until leakage. The crack propagation rate is calculated based on crack deformation, which is simulated by a two-way coupled mechanical finite-element method and dynamic fluid flow simulation.

The laminar simulation model presented in [14] was adapted for the application to three-dimensional parts. The flow model simulates the fluid flow as one-dimensional laminar flow using the electronic-hydraulic analogy. The fluid flow is assumed to be purely one-dimensional. The only significant flow is in the direction of the crack's advancement. The flow in other directions is negligible. However, this assumption is valid only for pure plane strain conditions when the part's size in the z-direction is considerably larger compared to the other dimensions. For a three-dimensional case, this holds true if the crack's width is considerably larger than the length and height

of the crack. While the crack's height is typically at least three orders of magnitude smaller than the crack's width, this is not always true for the crack's length. In cases of well established cracks, the crack's length can be in the same order of magnitude as the crack's width. However, in our case, the crack's length was limited to the wall thickness of the test specimens and therefore significantly smaller than the crack's width. In consequence, supplying the center line's deformation to the simulation was sufficient, and no modification to the fluid equations was required.

The crack is divided into  $N$  discrete sections with subscript  $i$  along its length (x-coordinate). Each section has a certain volume  $V_i(t)$ , density  $\rho_i(t)$ , pressure  $p_i(t)$  and crack opening displacement (height)  $h_i(t)$ . The volume flow between section  $i$  and  $i + 1$  is  $Q_i(t)$ , see Figure 3.

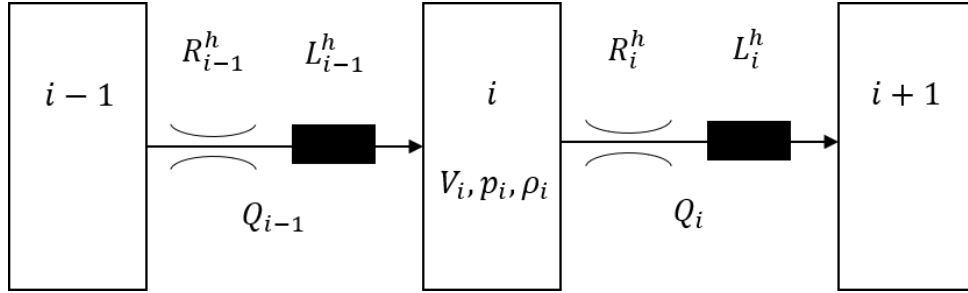


Figure 3: Fluid flow between discrete sections  $i - 1$ ,  $i$ , and  $i + 1$ , [14].

According to [14] the volume flow  $Q_i(t)$  between two sections can be calculated as

$$\begin{aligned} Q_i(t_k) &= \hat{Q}_i(t_k) - [\hat{Q}_i(t_k) - Q_i(t_{k-1})] e^{-\frac{\Delta t}{\tau_i}} \\ &= \hat{Q}_i(t_k) \left(1 - e^{-\frac{\Delta t}{\tau_i}}\right) + Q_i(t_{k-1}) e^{-\frac{\Delta t}{\tau_i}} \end{aligned} \quad (1)$$

with

$$\hat{Q}_i(t = t_k) = \frac{1}{R_i^h(t)} (p_i(t) - p_{i+1}(t)), \quad (2)$$

and the time factor  $\tau_i$  defined as

$$\tau_i(t) = \frac{L_i^h(t)}{R_i^h(t)}. \quad (3)$$

The hydraulic resistance  $R_i^h(t)$ , inductance  $L_i^h(t)$  and capacity  $C_i^h$  are defined as

$$R_i^h(t) = \left(12\eta \frac{l_i}{b h_i(t)^3}\right), L_i^h(t) = \rho_i(t) \frac{l_i}{b h_i(t)}, C_i^h = \frac{1}{K} l_i \cdot h_i(\mathbf{p}(t_k)) b, \quad (4)$$

with section length  $l_i$ , section width  $b$  and the fluids bulk module  $K$ .

In consequence, the mass balance leads to the volume change in section  $i$ ,

$$\begin{aligned} \Delta V_i(t_k) &= V_i(t_k) - V_i(t_{k-1}) \\ &= \left[ \frac{\rho_{i-1}}{\rho_i} Q_{i-1}(t_k) - Q_i(t_k) \right] \Delta t, \end{aligned} \quad (5)$$

and the pressure change

$$\begin{aligned} \Delta p_i(t_{k+1}) &= p_i(t_{k+1}) - p_i(t_k) \\ &= \frac{1}{C_i^h(t_k)} (\Delta V_i(t_k) - \Delta h_i(t_k) b l_i). \end{aligned} \quad (6)$$

The second part of eq. (6) is the volume change of the section due to the structural deformation  $\Delta h_i(t_k)$ :

$$\Delta h_i(t_k) = h_i(\mathbf{p}(t_k)) - h_i(\mathbf{p}(t_{k-1})). \quad (7)$$

The crack's opening displacement  $h_i(\mathbf{p}(t))$  equals the structural deformation. Under the assumption of an ideal-linear elastic material, the crack's opening displacement can be defined as

$$\mathbf{h}(\mathbf{p}(t)) = \mathbf{b} p_0(t) + \mathbf{A} \mathbf{p}(t), \quad (8)$$

with stiffness matrix  $\mathbf{A}$ . The coefficients of the stiffness matrix  $\mathbf{A}$  depend on the structural resistance and can be derived for a known pressure load and deformation. For  $N$  discrete sections,  $N$  independent pressure profiles and the corresponding deformation are required. A lower triangular matrix with arbitrary pressure satisfies this requirement, [14],

$$\begin{aligned} \mathbf{P} &= [\mathbf{p}^1 \quad \mathbf{p}^2 \quad \dots \quad \mathbf{p}^{N-1} \quad \mathbf{p}^N] \\ &= \begin{bmatrix} p & p & \dots & p & p \\ 0 & p & \dots & p & p \\ \vdots & \vdots & \ddots & \vdots & \vdots \\ 0 & 0 & \dots & 0 & p \end{bmatrix} \end{aligned} \quad (9)$$

with the corresponding deformation matrix  $\mathbf{H}$ :

$$\begin{aligned} \mathbf{H} &= [\mathbf{h}^1 \quad \mathbf{h}^2 \quad \dots \quad \mathbf{h}^{N-1} \quad \mathbf{h}^N] \\ &= \begin{bmatrix} h_1^1 & h_2^1 & \dots & h_{N-1}^1 & h_N^1 \\ h_1^2 & h_2^2 & \dots & h_{N-1}^2 & h_N^2 \\ \vdots & \vdots & \ddots & \vdots & \vdots \\ h_1^N & h_2^N & \dots & h_{N-1}^N & h_N^N \end{bmatrix} \end{aligned} \quad (10)$$

Inverting eq. (8) leads to the stiffness matrix  $\mathbf{A}$  as:

$$\mathbf{A} = \mathbf{P}^{-1} \mathbf{H}. \quad (11)$$

The stiffness matrix  $\mathbf{A}$  does not take into account the deformation of the crack due the external loads  $p_0(t)$ , which depends on the vector  $\mathbf{b}$  with shape  $N \times 1$ . The vector  $\mathbf{b}$  is determined accordingly to eq. (11) when only an external pressure  $p^e$  with corresponding crack deformation  $\mathbf{h}^0$  is applied, [14]:

$$\mathbf{b} = \mathbf{h}^0 / p^e. \quad (12)$$

As the crack advances, the structural stiffness of the specimen changes, as does the stiffness matrix  $\mathbf{A}$  and vector  $\mathbf{b}$ . Specific stiffness matrices and vectors were determined over the crack's advancement.

The 1D-coupled FSI simulates the pressure distribution and the structural stress levels of the test part as a temporal sequence. The minimum and maximum stress during one cycle give the required stress amplitude for the NASGRO equation. The NASGRO equation is based on the crack growth equations according to Erdogan/Ratwani [15] and Forman/Mettu [16]. In contrast to the commonly used Paris Equations, it takes directly into account the load ratio  $R$ :

$$R = \frac{\sigma_{min}}{\sigma_{max}} = \frac{K_{min}}{K_{max}}. \quad (13)$$

Following [1], we approximate the stress intensity factor  $K_I$  in relation to the crack's opening displacement.

$$K_I = \lim_{r \rightarrow 0} \frac{E}{(\kappa + 1)(1 + \nu)} \cdot \sqrt{\frac{2\pi}{r}} \cdot v. \quad (14)$$

The distance to the crack tip  $r = l_0 - x_i$  and for plain strain conditions,  $\kappa = \frac{3-\nu}{1+\nu}$ . The Poisson's ratio  $\nu$  for most metals can be approximated as  $\nu \approx 0.3$ .

However, at the crack tip ( $r = 0$ ),  $K_I$  cannot be calculated. Even in the vicinity of  $r = 0$  the numeric solutions degrade and low accuracy is reached. As a result, for  $r \rightarrow 0$ , the stress intensity factor is approximated with a linear regression.

Given the strain field  $v(x_i, t) = \frac{1}{2} h_i(t) \forall x_i \in [0, l_0]$ , the stress intensity function  $\tilde{K}_I(r)$  is calculated as

$$\tilde{K}_I(r) = \frac{E}{(4-\nu)} \cdot \sqrt{\frac{2\pi}{r}} \cdot v(l_0 - r). \quad (15)$$

$f(r) = m \cdot r + K_I$  is the linear regression of the numeric stress intensity factors, with the intercept being the approximate stress intensity factor  $K_I$ . The linear regression is solved with a least-squares approximation as

$$\begin{bmatrix} K_I \\ m \end{bmatrix} = \begin{bmatrix} 1 & \dots & 1 \\ r_1 & \dots & r_i \end{bmatrix}^{-1} \begin{bmatrix} \tilde{K}_I(r_1) \\ \vdots \\ \tilde{K}_I(r_i) \end{bmatrix}, \quad (16)$$

for  $r_i \in [0.1, 5] \text{ mm}$ .

For each time step  $t_i$ , the stress intensity factor is approximated, and the stress amplitude is calculated as the difference between the lowest and highest stress intensities,

$$\Delta K_I = K_{1,max} - K_{1,min}. \quad (17)$$

The NASGRO-Equation follows as

$$\frac{da}{dN} = C_{FM} \cdot \left[ \left( \frac{1-\gamma}{1-R} \right) \cdot \Delta K_I \right]^n \cdot \frac{\left( 1 - \frac{\Delta K_{1,th}}{\Delta K_I} \right)^p}{\left( 1 - \frac{K_{1,max}}{K_{1C}} \right)^q} \quad (18)$$

with material constants  $C_{FM}$ ,  $n$ ,  $\Delta K_{1,th}$ ,  $K_{1C}$ ,  $p$ , and  $q$ . The function  $\gamma(R)$  depends on the stress ratio  $R$  and is calculated as

$$\gamma = \max(R, A_0 + A_1 R + A_2 R^2 + A_3 R^3) \quad (19)$$

with coefficients

$$\begin{aligned} A_0 &= (0.825 - 0.34\alpha + 0.05\alpha^2) \cdot \cos\left(\frac{\pi}{2} S_R\right)^{1/\alpha}, \\ A_1 &= (0.415 - 0.071 * \alpha) \cdot S_R, \\ A_2 &= 1 - A_0 - A_1 - A_3, \\ A_3 &= 2A_0 + A_1 - 1, \end{aligned}$$

which in turn depend on the material constants  $\alpha$  and  $S_R$ .

All material constants were obtained from the NASGRO database, [17], except for  $C_{FM}$  and  $n$ , which were determined based on our experiments. The list of the used material constants is given in Table 1.

Table 1: NASGRO Material constants, unit system  $MPa\sqrt{(mm)}$

	$C_{FM}$	$n$	$p$	$q$	$\Delta K_{1,th}$	$K_{1C}$	$\alpha$	$S_R$
S235	$0.605E - 12$	2.65	0.5	0.5	243	2432	2	0.3

### 3 Experimental Setup

The objective of the test design was to create a test setup where stable crack growth is enforced while ensuring failure of the specimens after a reasonable number of cycles. In order to increase the statistical significance of the experiments, a flow divider was designed to process four specimens synchronously. Table 2 gives the load parameters of the performed experiments, except for the last parameter setup, Run 4, which was twice performed with 2 and 4 test specimens (6 in total). The three other runs were performed with four test specimens.

Table 2: Load parameters of the performed experiments.

Run	No. parts	Frequency	Pressure	Rise Time	Drop Time
1	4	3 Hz	400 bar	10 ms	40 ms s
2	4	3 Hz	400 bar	10 ms	5 ms s
3	4	6 Hz	400 bar	10 ms	80 ms s
4	6	6 Hz	400 bar	10 ms	5 ms s

#### 3.1 Test specimens

The part used for the experiments consisted of a hydraulic chamber with a defined notch to provoke favorable conditions for stable crack growth. The third direction of the part is extended to reduce the parasitic effects of the lateral edges and to attain two-dimensional fluid flow and plain strain conditions at the center of the notch. Figure 4 shows a cutaway drawing of the specimen and the complete assembly. The wall thickness at the notch is  $5 \text{ mm}$  limiting the crack's length to  $5 \text{ mm}$  before leakage of the specimens.

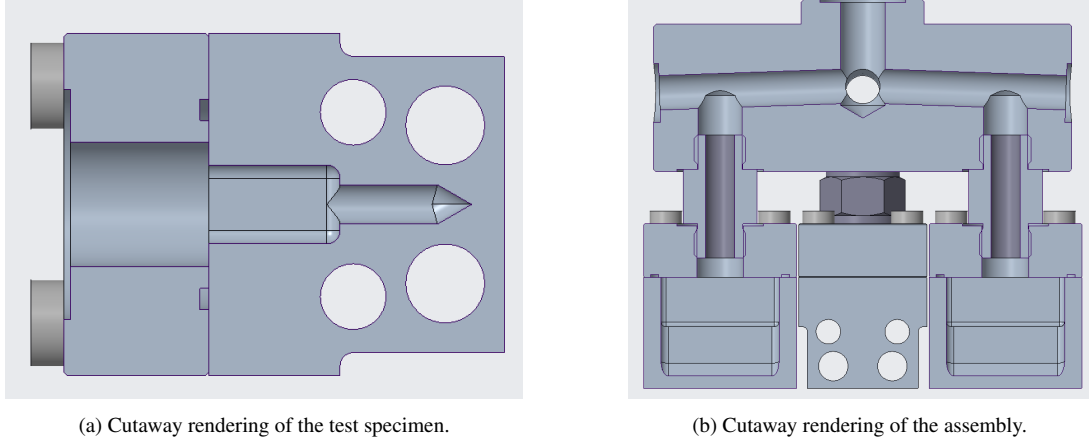


Figure 4: Test specimen and assembly design.

In total, one batch of 24 pieces was manufactured. To minimize variance due to different material treatments, each batch was made from the same batch of material. The base materials were rectangular extruded profiles of S235 steel. The parts were milled to the final geometry in two steps. At first, the shape and the inner pressure chamber were milled with standard milling tools. Following that, the notches were milled with a special tool to introduce a sharp edge and a predefined crack initiation ( $D = 6 \text{ mm}$ ,  $\alpha = 60^\circ$ ,  $R < 0.5$ ). Each test specimen was fixed with four M10 screws to an adapter plate with a G1/2" thread. The adapter plate was required as the G1/2" thread could not be integrated in the test specimens due to the manufacturing process of the notch. The assembled specimens were connected to a flow divider base with hydraulic fittings, as shown in Figure 5b. Compared to the total oil volume of the test specimens, the base assembly is characterized by large cross-sections to minimize pressure loss of the inflow and to avoid parasitic frequency dependencies in the inflow due to the flow resistance of the flow division.

### 3.2 Test bench

A simplified hydraulic scheme of the test bench is shown in Figure 5a, auxiliary components are omitted. Figure 5b shows the complete assembly with four mounted test specimens inside the test chamber. The pressure is supplied by a constant flow source. The high pressure level is controlled by a variable pressure relief valve. A variable throttle valve situated before the pulse generator controls the pressure build-up rate. A second throttle valve controls the pressure drop rate. One separable pressure sensor is included in the pulse generator, with another one located directly at the flow divider connected to the test specimens. The pulse generator creates a rectangular pressure pulsation at a variable frequency. The shape of the rectangular pulse, however, is constant with equal duration for the high and low pressure phases. Therefore, the maximum discharge time is limited to one-half of the pulse duration.

Due to the variable throttle valve, the pressure buildup and drop rate are typical charge/discharge curves. The discharge is approximated as

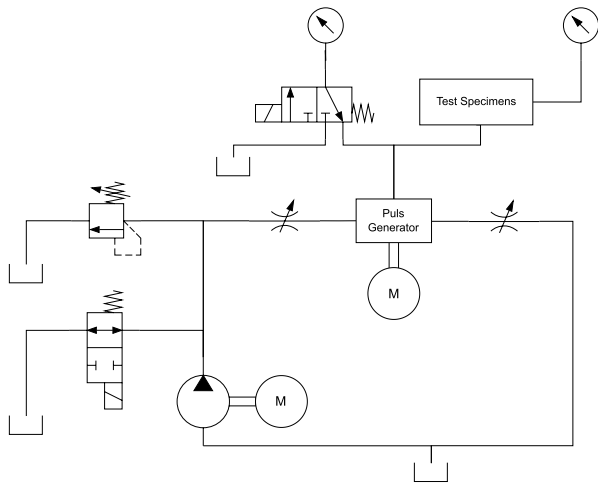
$$p(t) = p_0 e^{-\frac{2dp^-}{p_0} t}, \quad (20)$$

with average pressure drop rate  $dp^-$ . The inlet pressure pulsation at a frequency of  $3 \text{ Hz}$  for an average pressure drop rate of  $dp^- \approx 10 \text{ kbar/s}$  can be seen in Figure 6. The maximum pressure drop rate during discharge is  $dp_{max} = 2 dp^-$ .

The experiment is stopped by a float switch when the leaked oil quantity exceeds a particular threshold, which is roughly  $0.5 \text{ cm}^3$ . The specimens have failed in all cases as expected through leakage at the center of the face opposite of the notch. Additional, parasitic crack paths have not been noted in the experiments.

## 4 Results

In Figure 7 exemplary results of the fluid flow simulation are shown. The fluid pressure at the crack mouth followed the load pressure, while the crack tip pressure increased during the pressure drop to prevent the crack from closing completely. The crack's opening displacement at the crack mouth and the crack tip, see Figure 7b decreases largely but does, however, not attain zero. The lowest stress intensity factor is reached just at the reopening of the crack due to the increasing load pressure. The crack's opening displacement in relation to the distance to the crack tip



(a) Simplified hydraulic schematics of the test bench.



(b) Flow divider with four test specimens and a mounted pressure sensor.

Figure 5: Test bench and assembly.

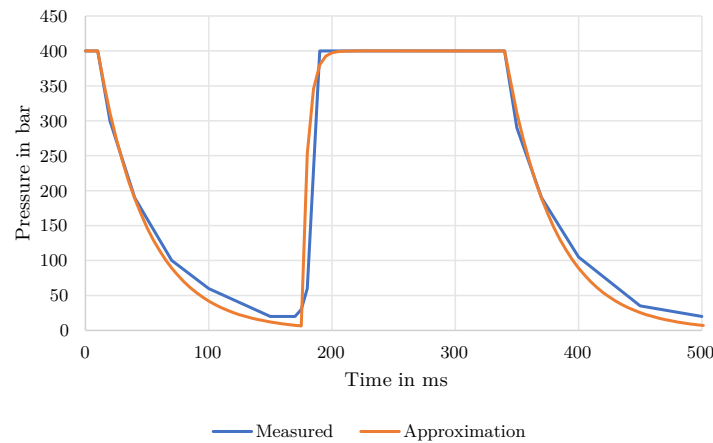


Figure 6: Inlet pressure pulse at 3 Hz and an average pressure drop rate of 5 kbar/s.

at the time of the lowest stress intensity factor is shown in Figure 7c. The crack mouth had already reopened, causing the pressure inside the crack to rapidly decrease. The crack's mouth was still filled with oil, maintaining a certain deformation, but the influence of the reopening crack mouth did not yet play a significant role. The stress intensity factor could not be calculated directly at the crack tip and was therefore approximated with a linear regression around the crack tip, see 7c. The stress intensity factor reached its maximum when the load pressure was established inside the crack, see 7d. As the load pressure was released, the pressure at the crack tip increased. The stress intensity factor, however, did not increase as the crack's opening displacement was decreasing.

As the crack advanced, two superposed effects were playing a role. On the one side, the structural resistance of the specimens decreased, and on the other side, the fluid-structure interaction plays a more important role as the crack's length increased. The reduced structural resistance led to a higher deformation, and, as a consequence, the maximal stress intensity factor increased, see Figure 8. On the other hand, the fluid-structure interaction had two effects. The pressure on the crack faces caused an additional load, increasing the structural deformation even further. Secondly, with increasing crack lengths, more oil was trapped in the crack as the load pressure was released, preventing the crack from closing and increasing the minimal stress intensity factor. As a consequence, the stress intensity factor's amplitude did not increase by the same amount as its maximum. The significance of this second effect increased with increasing load frequency.

The simulations show a significant influence of the pulse frequency on the crack growth rate and, therefore, the predicted lifetime. In Figure 9a the theoretical crack growth is compared for different frequencies and drop rates. One simulation was conducted under the assumption that no oil penetrates the crack (No FSI). In this case, the crack growth was considerably slower, and more cycles were required for the part to fail. When cracks were

filled with pressurized oil, the stress amplitude increased due to the pressure on the crack faces, and the cracks grew faster. However, when oil penetrated the cracks, the crack growth slowed down with increasing frequency. The crack advancement compared to the pulse count is shown in Figure 9b. The crack length was limited by the wall thickness of the specimens, which was 5 mm. The expected lifetime of the component increased at higher

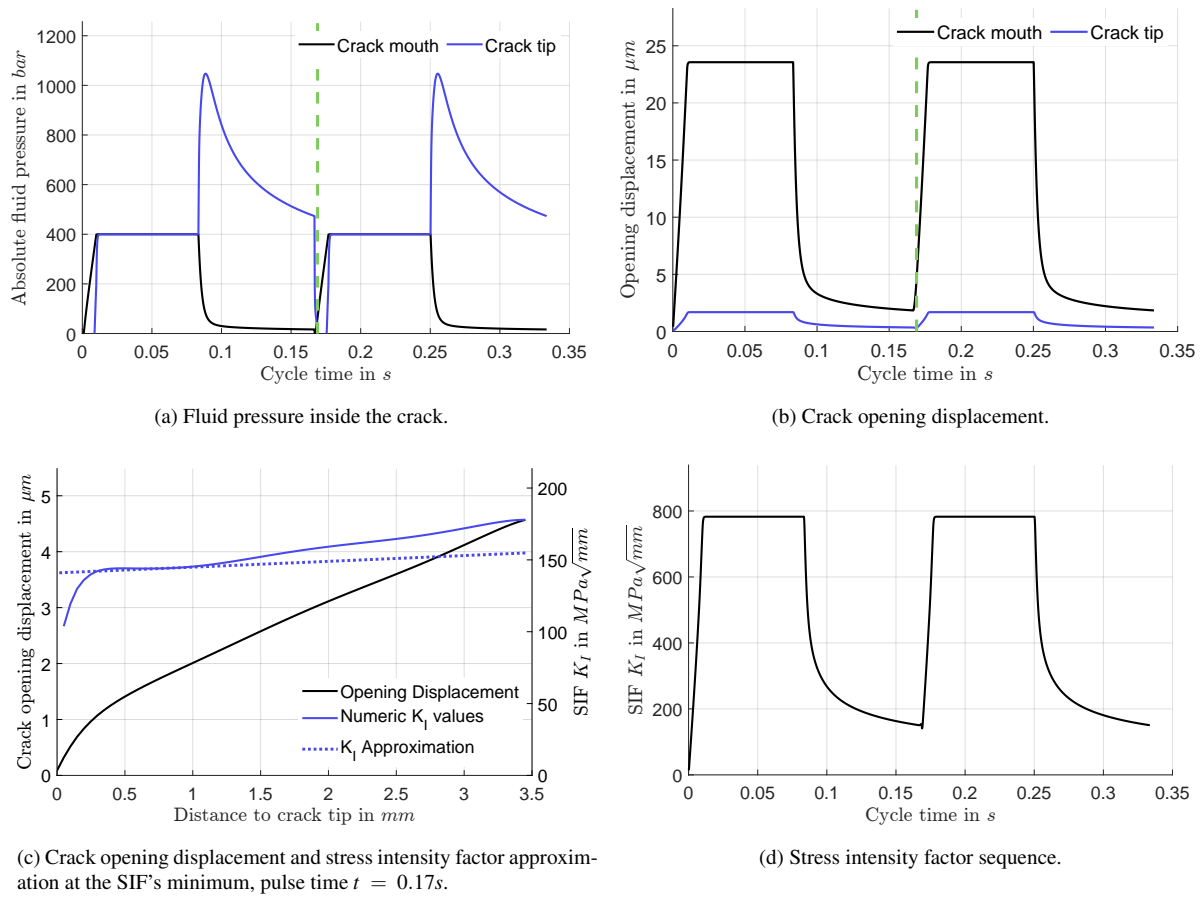


Figure 7: Simulation results for one pulse at a crack's length of 3.5 mm for a load frequency of 6 Hz with a drop rate of 80 kbar/s.

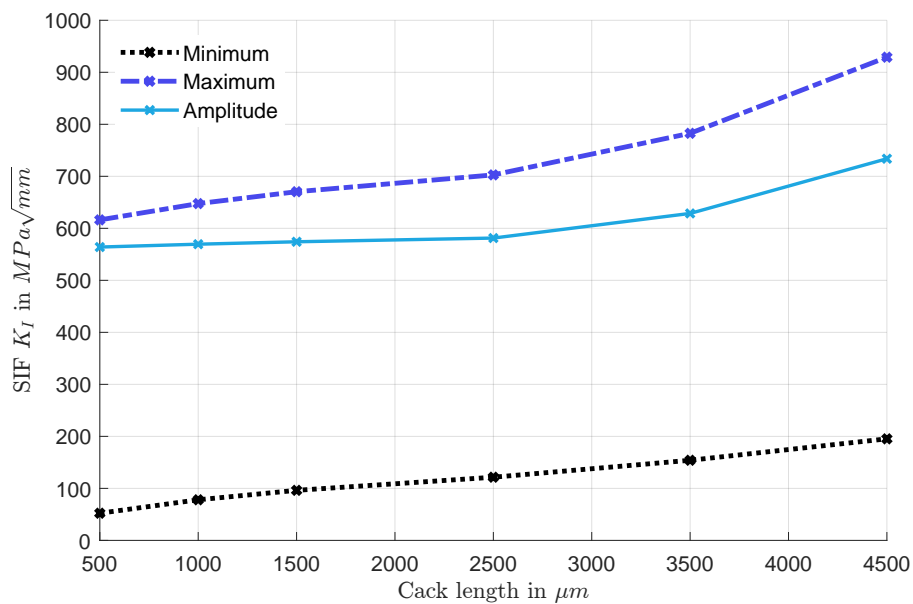


Figure 8: Simulated evolution of the minimal, maximal stress intensity factor, and its amplitude for a load frequency of 6 Hz with a drop rate of 80 kbar/s.

frequencies, whereas the drop rate did not have a significant influence except for a frequency of 12 Hz, where the discharge time of 10kbar/s was not sufficient for a complete discharge of the test specimens.

The results of the experiments, however, diverged from the expected behavior based on the simulations. In Figure 10 the crack growth for all four parameter setups is displayed. Due to the nature of the experiments, there was a certain spread between identical specimens. The time until a crack was initiated is one cause for a certain spread between identical specimens. To reduce the crack initiation lifetime, an artificial surface defect was introduced at a notch with a high stress concentration. The exact crack initiation could, however, not be measured in the experiment. The student's t-test was used to calculate the significance level of both sample distributions. The hypothesis that higher drop rates increase the lifetime of the test specimens achieved a significance level of 89 % at 3 Hz and 86% at 6 Hz. Regarding the frequency dependency, however, a significance level of 75 % was reached for the assumption that the lifetime is equal for the experiments with a drop rate of 80 kbar/s at 3 Hz and 6 Hz.

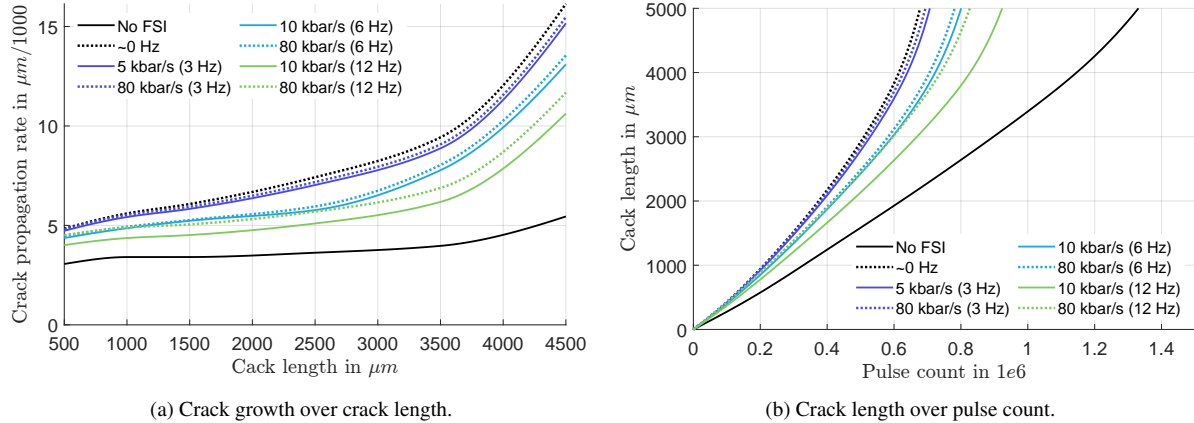


Figure 9: Simulated crack growth without fluid-structure interaction (No FSI) and with fluid-structure interaction for frequencies between 0 to 12 Hz and drop rates of 5, 10, and 80 kbar/s.

The results of the fatigue simulation are in line with the expectations based on previous studies. While most studies agree that hydraulic fatigue is time dependent, not all implications are fully understood. The proposed fatigue simulation offers a simple and time-effective method to predict fatigue for elementary geometries. However, the performed experiments do not align with the results of the simulation. A time dependency can be stated in both the experiments and the simulation. The statistical confidence levels support the assumption of a systematic time dependency in the experiments. Unpredicted is, however, the magnitude of the life-time difference for 5 kbar/s and 10 kbar/s as well as the lack of a deviation regarding the frequency. A possible explanation could be that the simulated oil trapping is overlaid with other effects, e.g. crack closure, which prevents the oil from flowing out and therefore limits the frequency dependency in favor of the drop rate. Another assumption is that one or more competing effects that influence the lifetime are superposed with the simulated effect. Additionally, crack closure and incompatibility of crack faces can prevent crack closure and provoke deformation of the unloaded pieces, even without oil trapping. These effects, however, cannot account for the drop rate dependence of crack growth. The reason for these results and whether the drop rate dependency can be repeated with different geometries should be studied in further experiments.

## 5 Conclusion

In this paper, we presented a fatigue prediction based on a numeric fluid flow simulation that accounts for fluid-structure interactions and is able to predict a frequency dependency of the hydraulic lifetime. Fluid dynamics and flow resistance are respected, showing that fluid flow inside fatigue cracks leads to oil trapping. At higher frequencies, the oil is not able to flow out of the crack during the discharge phase of the pulsation, and the remaining oil prevents crack closure. Without crack closure, the crack tip remains under stress, and the overall mechanical stress amplitudes are reduced. In consequence, the crack advancement per cycle decreases and the specimen's lifetime increases. In addition, special test specimens with an elementary geometry have been designed to enforce stable crack growth. On a hydraulic test bench, a pressure pulse was applied to the test specimens until leakage occurred. The number of cycles until leakage was compared to simulation. Contrary to the simulation, the dominant parameter in the experiments has not been the pulse frequency but the drop rate of the pulse. There are a couple of possible explanations for the different behavior of the experiments compared to the theory. The fluid-flow interaction is limited to straight laminar flow and does not account for roughness or surface effects, which we assume to have a possible influence on the crack growth. In further studies, the crack growth has to

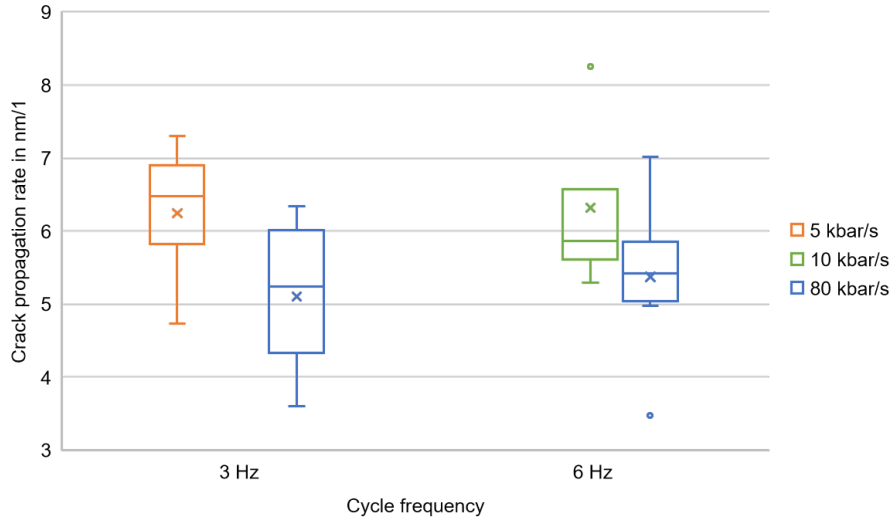


Figure 10: Cycles until leakage, the box extends from the lower to the upper quartile with median line and mean. Outliers are at least 1.5 times the interquartile range smaller/larger than the extent of the box.

be measured during the experiments to directly compare the crack growth rate. A destructive measurement of the crack length would require new test specimens, as the experiment could not be continued with the same specimens after the measurement. The possible alternative to measuring the crack length would be to measure the mechanical deformation of the test specimens during the experiments. The mechanical deformation on one side shows the crack advancement, while on the other, it can be used to verify the assumption that oil remains trapped inside the crack. If the fluid-structure interaction introduces a frequency dependency, this property could be exploited even further to monitor crack growth and for non-destructive detection of cracks. In theory, trapped oil should cause a phase difference between the fluid load pressure and the structural deformation. Measuring the deformation with high-precision optical techniques could possibly be used as a non-destructive method for crack detection inside hydraulic components.

## Acknowledgements

This work was funded by the German Research Foundation (DFG) under project number 449676223.

## Nomenclature

Designation	Denotation	Unit
$p$	Pressure	$Pa$
$dp^-$	Pressure drop rate	$Pa/s$
$V$	Volume	$m^3$
$Q$	Volume flow	$m^3/s$
$\rho$	Density	$kg/m^3$
$R^h$	Hydraulic Resistance	$Pa/m^3$
$L^h$	Hydraulic Inductance	$(Pa \cdot s)/m^3$
$C^h$	Hydraulic Capacity	$m^3/Pa$
$l$	Length	$m$
$b$	Width	$m$
$h$	Height / Size / Crack opening	$m$
$r$	Crack tip radius	$m$
$E$	Young's modulus	$Pa$
$K$	Bulk modulus	$Pa$
$\nu$	Poisson's ratio	—
$K_I$	Stress Intensity Factor	$MPa\sqrt{mm}$
$R$	Stress Ratio	1

## References

- [1] Hans Albert Richard and Manuela Sander. *Fatigue Crack Growth*, volume 227 of *Solid Mechanics and Its Applications*. Springer International Publishing, Cham, 2016.
- [2] A Crook. The Effect Of Cyclic Test Frequency on the Fatigue Life of Fluid Power Components. In *7th International Fluid Power Symposium*, Bath, September 1986.
- [3] F. H. Davis, E. G. Ellison, and W. J. Plumbridge. Effects of Hydrostatic Pressure on the Rate of Fatigue Crack Growth. *Fatigue & Fracture of Engineering Materials & Structures*, 12(6):511–525, 1989.
- [4] F. H. Davis and E. G. Ellison. Hydrodynamic Pressure Effects of Viscous Fluid Flow in a Fatigue Crack. *Fatigue & Fracture of Engineering Materials & Structures*, 12(6):527–542, 1989.
- [5] W. J. Plumbridge, P. J. Ross, and J. S. C. Parry. Fatigue crack growth in liquids under pressure. *Materials Science and Engineering*, 68(2):219–232, January 1985.
- [6] C. J. Polk, W. R. Murphy, and C. N. Rowe. Determining Fatigue Crack Propagation Rates in Lubricating Environments through the Application of a Fracture Mechanics Technique. *A S L E Transactions*, 18(4):290–298, January 1975.
- [7] J.L. Tzou, S. Suresh, and R.O. Ritchie. Fatigue crack propagation in viscous environments. In J. CARLSSON and N.G. OHLSON, editors, *Mechanical Behaviour of Materials*, pages 711–717. Pergamon, January 1984.
- [8] D. I. Fletcher, P. Hyde, and A. Kapoor. Modelling and full-scale trials to investigate fluid pressurisation of rolling contact fatigue cracks. *Wear*, 265(9):1317–1324, October 2008.
- [9] Makoto Akama and Tadao Mori. Boundary Element Analysis of Effects of Crack Face Friction and Trapped Fluid on Rolling Contact Fatigue Cracks. *Quarterly Report of RTRI*, 46(4):231–237, 2005.
- [10] R. Bourga, P. Moore, Y. J. Janin, B. Wang, and J. Sharples. Leak-before-break: Global perspectives and procedures. *International Journal of Pressure Vessels and Piping*, 129–130:43–49, May 2015.
- [11] N M Bagshaw, S B M Beck, and J R Yates. Identification of fluid flow regimes in narrow cracks. *Proceedings of the Institution of Mechanical Engineers, Part C: Journal of Mechanical Engineering Science*, 214(8):1099–1106, August 2000.
- [12] L. V. Clarke, H. Bainbridge, S. B. M. Beck, and J. R. Yates. Measurement of fluid flow rates through cracks. *International Journal of Pressure Vessels and Piping*, 71(1):71–75, April 1997.
- [13] Lukas Michiels and Marcus Geimer. Influence of High Pressure Drop Rates on Fatigue Crack Growth. *Chemical Engineering & Technology*, September 2022.
- [14] Lukas Michiels and Marcus Geimer. Dynamic fluid simulation of hydraulic oil flow inside fatigue cracks during transient loads. In *Proceedings of 7th Global Fluid Power Society PhD Symposium (GFPS 2022)*, Naples, 2022.
- [15] F. Erdogan and M. Ratwani. Fatigue and fracture of cylindrical shells containing a circumferential crack. *International Journal of Fracture Mechanics*, 6(4):379–392, December 1970.
- [16] Royce G. Forman and Sambhi R. Mettu. Behavior of surface and corner cracks subjected to tensile and bending loads in Ti-6Al-4V alloy. Technical Report S-611, September 1990.
- [17] Southwest Research Institute. APPENDIX A - NASGRO 3.0 MATERIALS CONSTANTS, 2022.